Liu, Y.; Gould, O.; Kratz, K.; Lendlein, A.:
Shape-Memory Actuation of Individual Micro-/Nanofibers.
In: MRS Advances. Vol. 5 (2020) 46 - 47, 2391 - 2399.
First published online by Cambridge University Press: 18.06.2020

https://dx.doi.org/10.1557/adv.2020.276

Shape-Memory Actuation of Individual Micro-/Nanofibers

Yue Liu[1,2], Oliver E. C. Gould[1], Karl Kratz[1], Andreas Lendlein[1,2]

[1] Institute of Biomaterial Science, Helmholtz-Zentrum Geesthacht, Kantstr. 55, 14513 Teltow, Germany

[2] Institute of Chemistry, University of Potsdam, 14476 Potsdam, Germany

*Correspondence to: Prof. Andreas Lendlein, e-mail: andreas.lendlein@hzg.de

ABSTRACT

Advances in the fabrication and characterization of polymeric nanomaterials has greatly advanced the miniaturization of soft actuators, creating materials capable of replicating the functional physical behavior previously limited to the macroscale. Here, we demonstrate how a reversible shape-memory polymer actuation can be generated in a single micro/nano object, where the shape change during actuation of an individual fiber can be dictated by programming using an AFM-based method. Electrospinning was used to prepare poly(ε-caprolactone) micro-/nanofibers, which were fixed and crosslinked on a structured silicon wafer. The programming as well as the observation of recovery and reversible displacement of the fiber were performed by vertical three point bending, using an AFM testing platform introduced here. A plateau tip was utilized to improve the stability of the fiber contact and working distance, enabling larger deformations and greater rbSMPA performance. Values for the reversible elongation of ε_{rev} = 3.4 ± 0.1% and 10.5 ± 0.1% were obtained for a single micro (d = 1.0 ± 0.2 µm) and nanofiber (d = 300 ± 100 nm) in cyclic testing between the temperatures 10 and 60 °C. The reversible actuation of the nanofiber was successfully characterized for 10 cycles. The demonstration and characterization of individual shape-memory nano and microfiber actuators represents an important step in the creation of miniaturized robotic devices capable of performing complex physical functions at the length scale of cells and structural component of the extracellular matrix.

INTRODUCTION

Micro-/nanoscale polymeric devices capable of stimuli-responsive actuation are highly sought after for applications in sensors [1], medicine [2, 3], and microfluidics [4], where the ability to sense and reversibly react to changes in the external environment is important for achieving autonomous functional behavior [5]. Among the wide variety of previously demonstrated micro-/nanoscale morphologies [6, 7], the highly scalable nature of fiber production has made polymeric fibers capable of dynamic shape change popular for the creation of artificial muscles, biosensors, and wearable devices [8, 9]. The implementation of

a shape-memory effect has enabled one-way programmable shape change without the presence of a solvent, and the exertion of stresses in the order of megapascals [5]. However, it has limited materials to a one-time transformation in geometry after each programming step, hindering the use in applications where a continuous response to alternating environmental conditions is needed. The recently developed two-way shape-memory polymer actuation imbues suitable materials with reversible, bidirectional movements between two programmable states [10]. The realization of a programmable reversible shape-memory actuation is dependent on the incorporation of two parts of crystalline domains within the material with one or two distinct thermal transitions. For materials with one broad thermal transition, crystalline domains below a separation temperature (T_{sep}) act as actuation domains, which undergo transitions between the solid/crystalline state and the melt during cooling to low temperature (T_{low}) and heating to T_{sep} that induce reversible elongation (ε_{rev}) toward a temporary shape. Those domains above T_{sep} will act as skeleton forming domains, forming a scaffold that guides the crystallization of the actuation domains.

The technological realization of micro-/nano-actuators requires both the implementation and characterization of actuation behavior, with the goal of controlling and quantifying the reversible shape-memory effect of a single micro/nano crystallizable fiber in terms of geometry change and force generation during actuation. For nanofibers, AFM three-point deformation testing, due to its high spatial resolution and force-sensing capabilities, is the most promising method for mechanical and shape-memory effect characterization [11]. In previous work, a universal atomic force microscopy (AFM) test platform enabled the realization of a one-way thermomechanically induced shape-memory effect for individual polymeric micro/nano systems [12]. A tipless cantilever was utilized to perform vertical loading on PEU fibers during programming and track the recovery process. The recovery of the original free-suspended micro-/nanofiber geometry with programming strains of 10 ± 1% and 21 ± 1% were realized upon heating.

Here, we advance this method to achieve the incorporation and characterization of a reversible shape-memory actuation capability into individual polymeric micro-/nanofibers. Crosslinked poly(ε-caprolactone) was chosen for investigation based on its excellent reversible shape-memory effect [13]. Micro-/nanofibers with different diameters were prepared by electrospinning, and fixed onto a structured silicon wafer substrate by UV glue. Using an adapted AFM-based technique we were able to both program and characterize the recovery and reversible movement of the fiber.

EXPERIMENTAL DETAILS

Preparation of electrospun fibers and fixation on silicon substrate

PCL fibers were fabricated by the electrospinning of a 15% w/v PCL/chloroform-ethanol solution with 2 wt% triallyl isocyanurate TAIC (≥99%) and 2 wt% Benzophenone BP (99%) as photocrosslinker. An electrical field was provided by a high voltage power supply (PNC 40000-1 ump; Heinzinger, Rosenheim, Germany). A stainless steel capillary with an outer diameter of 0.8 mm was connected to a 20 mL polyethylene syringe filled with 10 mL of solution. A constant volume flow rate was maintained using a syringe pump (Linari Engineering S.r.l., Italy). A rotating mandrel with the radius of 5 cm was connected as the collecting electrode. A structured silicon waferIMS (Chips, Stuttgart, Germany), composed of 30 µm squared pillars with 20 µm spacing, was used to

collect the fibers. For the fixation of the fiber on the structured wafer, acrylate based UV crosslink glue (Vitralit® 311, Panacol, Germany) was coated on the top surface of the structured silicon wafer before the collection of the electonspun fibers. The distance between the structured silicon wafer substrate fixed on the drum and the needle was 20 cm. An applied voltage of 15-25 kV, at a rotating speed of 1-10 rpm, and a mass flow rate of about 1.41 to 2.12 $mL \cdot h^{-1}$ was used to obtain a stable jet during electrospinning at ambient temperature. The prepared samples were then immediately exposed to UV light (Uniform Exposure System, ABET technologies, Milford, Connecticut) with a UV wavelength of 350-450 nm for 30 minutes to cure the glue and crosslink the fibers.

Electron microscopy

The morphology and size of PCL fibers were characterized by SEM. SEM imaging was carried out by an ESEM Quanta 250 FEG, on a sample without coating, in low vacuum mode (33 Pa), at 2 kV, and with a large field detector. The obtained SEM images were analyzed using ImageJ (version 1.44; National Institutes of Health). To determine the average diameter of cPCL microfibers approximately 10 single fibers on structured wafer were measured.

Atomic force microscopy

The programming and characterization of fibers was performed by a MFP-3D AFM (Asylum Research). Temperature control was achieved using an Environmental Controller (Asylum Research) with a Peltier element. The plateau tip cantilevers (SD-PL-NCH, Nanosensors, Germany) used for programming had a driving frequency of around 330 kHz and a spring constant of 42 N/m. The driving frequency and spring constant of plateau tip cantilevers (SD-PL-CONT, Nanosensors, Germany) used for the real-time investigation of fiber displacement were 13 kHz and 0.2 N/m. The geometry of the plateau tip was a blunt tip with a well-defined circular end-face (plateau diameter of 10 ± 0.1 µm and height of 15 ± 0.1 µm). The AFM height images of the micro- and nanofibers were obtained using a typical scanning rate of 1.0 Hz.

Programming and Fixing

A representative programming process of the microfibers is described here exemplarily. The temperature of the testing system was heated to T_{deform} = 80 ºC and equilibrated for 10 min. After obtaining a height image of a single microfiber, the plateau tip cantilever (SD-PL-NCH) was moved in order to locate the tip towards the midpoint of the microfilament. Then, the approach of the cantilever onto the microfilament was initiated with the set force of 25 µN and an integral gain of 0.01, while the real-time deflection and height (Z-piezo) data were collected by AFM. The microfiber's deformation was kept for 10 min before the temperature was reduced down to T_{low} = 10 ºC at 10 $ºC \cdot min^{-1}$ and equilibrated for another 10 min. Finally, the cantilever was withdrawn to release the load.

Actuation characterization

For the characterization of stress-free actuation, the fiber was heated to the separation temperature T_{sep} = 60 °C. The AFM tip, with the AFM in contact mode and using plateau tip cantilevers (SD-PL-CONT), was approached onto the midpoint of the temporarily deformed microfiber. After the scan size and integral gain were set to 0 and 0.01, the temperature was cycled between T_{sep} = 60 °C and T_{low} = 10 ºC at 5 ºC·min^{-1}. The real-time height (Z-piezo) data were collected by AFM. To exclude the thermal movement of the heater-cooler and tip holder, the background change of z-direction on the undeformed fiber between pillars with AC mode was recorded with 5 cycles of heating and cooling. All the cycles presented similar curves in displacement of z-direction versus temperature, indicating a stable background system.

RESULTS AND DISCUSSION

cPCL fibers were fabricated and fixed on a microstructured silicon wafer for investigation as shown in the schematic diagram (Figure 1a). A structured silicon wafer with a periodic array of micropillars on its surface was used to support the free-suspended microfibers prepared via electrospinning. The length, width, and height of each pillar were measured as 30.0 ± 0.1, 30.0 ± 0.1 and 15.0 ± 0.1 μm respectively, while the gap distance between two neighboring pillars was measured as 20.0 ± 0.1 μm. This structure was designed to facilitate larger strain values, according to the geometry of plateau tip. PCL fibers with diameters (d) of 2.1 ± 0.3 μm, 1.0 ± 0.2 μm, 0.3 ± 0.1 μm were prepared by electrospinning and deposited onto the top of the micropillars that was coated with UV glue. The structured silicon wafer and PCL fibers were then exposed to UV light for 30 minutes to crosslink the PCL fiber and cure the UV glue. After fixation, a lateral movement of the AFM cantilever was applied to the fiber between the pillars to stretch the fiber and check the displacement of the fixation part. The fixed fiber positions observed from optical microscopy did not vary, suggesting the firm attachment of fibers onto the pillars.

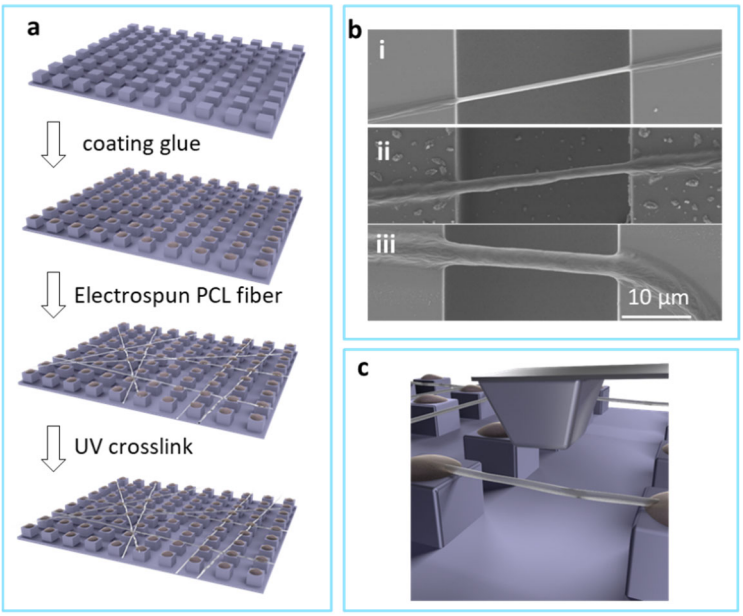

Figure 1 (a) Fabrication scheme: fixation of cPCL fibers on a microstructured silicon wafer (b) SEM image of cPCL fiber with different diameters of (i) 300 ± 50 nm, (ii) 1.0 ± 0.2 µm and (iii) 2.1 ± 0.3 µm. (c) Schematic illustrating the programming of a nanofiber through vertical bending

The thermal properties of the cPCL fibers were the subject of initial investigation, in order to identify suitable temperatures for the programming and reversible actuation of a suspended fiber. As reported previously, DSC measurements of cPCL fiber meshes showed a melting transition in the range of 35 °C - 63 °C and crystallization in the range of 40 °C - 12 °C, attributed to crystalline PCL domains [13]. The broad nature of this melting transition makes the crystalline PCL domains suitable for shape-memory actuation behavior, as it allows for the selective melting of a particular crystallite population [10, 14].

To program a suspend fiber, the temperature of the testing system was increased to a deformation temperature of T_{deform} = 80 °C, and equilibrated for 10 minutes to ensure the crystalline PCL domains were melted. Fibers that are individually suspended across the micropillars and parallel along the side of the square were chosen for investigation. The initial length of the free suspended part can be assumed as l_0 = 20 µm. An AFM scan in AC mode was performed to obtain a height image of a single microfiber and to locate the midpoint along the free-suspended fiber between the pillars for programming. A plateau tip (Figure 1c) was chosen to perform the deformation of the fibers for the following reasons. The plateau tip possesses a blunt tip with a well-defined circular end-face (plateau diameter of 10 ± 0.1 µm and height of 15 ± 0.1 µm) located at the free end of a micromechanical cantilever. The geometry of the plateau tip allowed a larger

contact area with the fiber to avoid slippage during temperature change induced drifting. In addition, the shape of the plateau tip is capable of providing larger deformations (~80% strain) when compared to tip-less cantilevers (capable of inducing ~10% strain), necessary to achieve pronounced actuation performance. An important requirement of the cantilever is that it must cause no considerable change in deflection during heating and cooling within the temperature range used for actuation and programming. Non-coated cantilevers were utilized to avoid a variation in thermal expansions between a metal coating layer and the silicon material of the cantilever.

The cantilever was engaged onto the fiber with a set force of 20 μN after being positioned at the midpoint of the fiber, while the integral gain was set to 0.01, to stabilize the speed of deformation (8.6 $nm \cdot s^{-1}$). After reaching the set force the system was equilibrated for 10 min. Fixation of the temporary elongated shape was achieved by cooling the deformed fiber down to 10 °C at a rate of 10 $°C \cdot min^{-1}$ and equilibrating for another 10 min. To release the external force after fixation, the cantilever was withdrawn and retracted back to its highest position. A height image of the programmed sample was then captured by scanning the sample in AC-mode at 10 °C, allowing for analysis of the fixed geometry. It was found that after the programming and fixation procedures, the microfiber (d = 1.0 ± 0.2 μm) was successfully deformed vertically and fixed at its temporary shape with a displacement (D_v = 7.7 μm) towards the surface between pillars. Assuming the contact line of plateau tip and fiber was l_c = 10 μm, the elongation of the fiber was calculated as l_e = 28.36 μm with a strain value ε of 41.8% using the following equations.

$$l_e = l_c + 2 * \sqrt{{D_v}^2 + (\frac{l_0 - l_c}{2})^2} \quad \text{Equation 1}$$

$$\varepsilon = \frac{l_e - l_0}{l_0} \quad \text{Equation 2}$$

To achieve reversible actuation, the programmed sample was then heated to a separation temperature (T_{sep} = 60 °C), initiating partial recovery to a length of 20.09 μm (D_v = 0.67 μm, ε = 0.88%). The same procedure was performed with a nanofiber (d = 300 ± 50 nm), which was successfully deformed vertically (D_v = 9.3 μm) and fixed in a temporary shape. The elongation of the nanofiber was calculated as 31.1 μm with a strain ε of 55.5%. The programmed nanofiber sample was then heated to separation temperature (T_{sep} = 60 °C) and the recovered fiber displacement was measured from cross-section profile of height image. Based on the calculation, the nanofiber underwent partial recovery to a length of 20.2 μm (D_v = 1 μm, ε= 1%).

The stress-free reversible actuation of a single free-suspended PCL micro-/nano-fiber was observed by reversibly heating and cooling between 60 °C and 10 °C. Height images of the micro-/nano-fibers were captured by AFM imaging in AC-mode at 60 °C and 10 °C, allowing the comparison of geometry change during actuation from the cross-section profile along the fiber. For the microfiber (d = 1.0 ± 0.2 μm), the length increased from 20.1 μm to 20.8 μm (D_v = 1.98 μm, ε= 3.8%) during cooling. The reversible elongated strain ε_{rev}, which was described by equations in previous work [14], was calculated as 2.9%. The length of the nanofiber (d = 300 ± 50 nm) was measured to change from 20.2 μm to 22.3 μm (D_v = 3.58 μm, ε= 11.5%) after cooling, and a reversible elongation change in strain of ε_{rev} = 10.5%. When heated to 60 °C again, the micro-/nanofiber recovered to

the length of 20.1 ± 0.1 and 20.2 ± 0.1 μm due to melting induced contraction. It can be assumed that the orientated crystallization of PCL domains during cooling resulted in the elongation of the single fiber, which needs further investigation between different scales.

The different molecular orientation and crystal structure of polymer chains in micro- and nano-fibers before programming were analyzed by AFM phase images. The cPCL fibers with diameter of 2.1 ± 0.3 μm, 1.0 ± 0.2 μm, 0.3 ± 0.1 μm were deposited on the flat silicon wafer surface and scanned with AFM by AC mode to acquire the height and phase images at room temperature (ca. 25 °C), as shown in Figure 2. It can be observed that the morphology of nanofibers with smaller diameters presented both densely packed aligned lamellae and fibrillar structures (Figure 2c). The amorphous regions in between mostly contained extended tie molecules which connect and lock the adjacent crystalline phases. In contrast, microfibers with larger diameters exhibited misaligned lamellae and the absence of fibrillar structures in the crystalline phase, as shown in Figure 2a. The amorphous regions consist of relaxed tie molecules that result in less resistance to the tensile force and disentangle during stretching. Therefore in this study, only in fibers diameter below 1 μm, crystallites are highly oriented along the nanofiber axis, as well as contain oriented fibrillar structures, determining the pronounced reversible elongation compared to the thick microfibers [15].

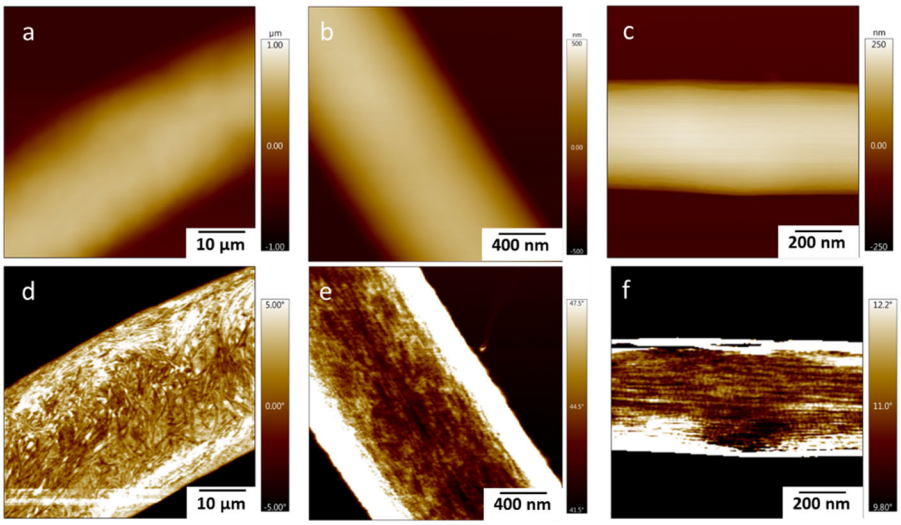

Figure 2 AFM height images (a-c) and phase images (d-f) of undeformed cPCL micro-/nanofibers with different diameters (a,d. 2.1 ± 0.3 μm, b, e. 1.0 ± 0.2 μm, c, f. 0.3 ± 0.1 μm) at 25 °C

The actuation performance of cPCL single fibers with diameters of 300 ± 50 nm were further explored in repetitive heating and cooling cycles between T_{sep} = 60 °C and T_{low} = 30 °C. A higher low temperature was chosen here to avoid the drifting effect induced hitting of the tip to the edge of micropillars, which would interrupt the tracking of fiber displacement during temperature changes. The observation of actuation was investigated as real-time fiber displacement performed with a plateau cantilever with a low spring constant (k = 0.2 N/m), giving higher sensitivity to the movement and force exerted by the fiber. The height variation of the background was measured on the undeformed fiber and subtracted

from the total values of displacement, which resulted in the displacement vs. temperature curves shown in Figure 3b. The displacement at low temperature was defined as 0 from the lowest point on the bended fiber and the recovery movement upwards during heating was recorded positive from the analysis. A stable reversible displacement at the mid-point of the nanofiber was recorded by the AFM plateau tip during 10 cycles alternating change in temperatures. Based on previous equations, the reversible elongation strain of 10 cycles was calculated as ε_{rev} = 10.5 ± 0.2%, indicating a stable shape-memory actuation behavior. Besides, an actuation induced pulling force of 0.2 ± 0.01 nN upon cooling and pushing force of 0.5 ± 0.1 nN during heating were detected on the tip. The actuation temperature, occuring at maximum velocity in changing dimensions were measured as 55.1 ± 0.2 °C during heating and 42.9 ± 0.2 °C upon cooling.

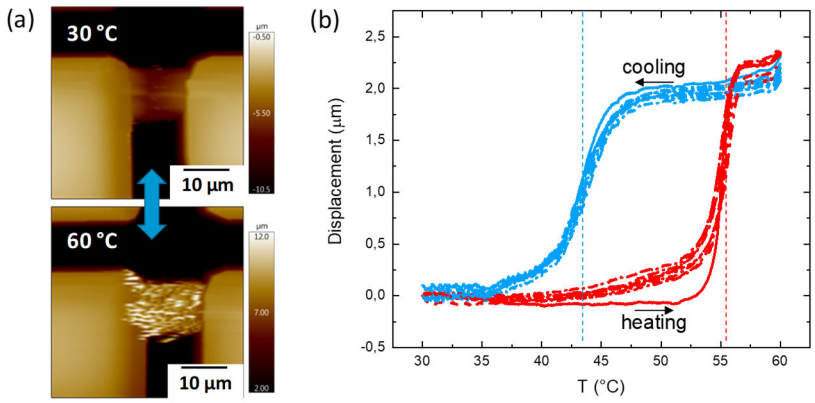

Figure 3 (a) AFM height images of fiber at 30 °C and 60 °C. (b) Reversible displacement during heating and cooling of cPCL nanofiber

CONCLUSION

In this paper we report on the implementation and characterization of a shape-memory actuation capability in a single isolated nano/microfiber by an AFM-based method. By refining the geometry of the substrate and using a plateau tip, large deformations of single PCL fibers necessary to generate a reversible actuation were achieved. The morphology of the suspended fibers was analysed with AFM phase imaging, where it was observed that fibers with diameters of 300 ± 50 nm exhibited both densely packed aligned lamellae and fibrillar structures. This high molecular alignment within the smaller fibers promoted the crystallization-induced elongation during cooling and resulted in a higher reversible effect, with a reversible strain change of ε_{rev} = 10.5% measured for the nanofibers as opposed to ε_{rev} = 2.9% measured for the microfibers (d = 1.0 ± 0.2 µm). Further, the stability of the actuation behavior of the nanofibers was demonstrated in measurements over ten cycles, where a variation of 0.2% in ε_{rev} was measured. By demonstrating the implementation and characterization of a

shape-memory actuation capability in nano and microfibers, a new range of miniaturized soft devices capable of dynamic and autonomous physical behavior might be enabled in the future.

ACKNOWLEDGMENT

This work was financially supported by the Helmholtz Association through programme-oriented funding and by the German Federal Ministry for Education and Research through the Programme Health Research (grant No. 031A095).

References

1. L. Hu, Q. Zhang, X. Li and M. J. Serpe, *Mater. Horiz.* **6** (9), 1774-1793 (2019).
2. B. Q. Y. Chan, Z. W. K. Low, S. J. W. Heng, S. Y. Chan, C. Owh and X. J. Loh, *ACS Appl. Mater. Interfaces* **8** (16), 10070-10087 (2016).
3. J. Zhou and S. S. Sheiko, *J. Polym. Sci., Part B: Polym. Phys.* **54** (14), 1365-1380 (2016).
4. J. M. Robertson, R. X. Rodriguez, L. R. Holmes, P. T. Mather and E. D. Wetzel, *Smart Mater. Struct.* **25** (8), 085043 (2016).
5. A. Lendlein and O. E. C. Gould, *Nat. Rev. Mater.* **4** (2), 116-133 (2019).
6. C. T. Lim, E. P. S. Tan and S. Y. Ng, *Appl. Phys. Lett.* **92** (14), 141908 (2008).
7. A. Baji, Y.-W. Mai, S.-C. Wong, M. Abtahi and P. Chen, *Compos. Sci. Technol.* **70** (5), 703-718 (2010).
8. L. Ionov, G. Stoychev, D. Jehnichen and J. U. Sommer, *ACS Appl. Mater. Interfaces* **9** (5), 4873-4881 (2017).
9. G. V. Stoychev and L. Ionov, *ACS Appl. Mater. Interfaces* **8** (37), 24281-24294 (2016).
10. M. Behl, K. Kratz, U. Noechel, T. Sauter and A. Lendlein, *Proc. Natl. Acad. Sci. U. S. A.* **110** (31), 12555-12559 (2013).
11. B. R. Neugirg, M. Burgard, A. Greiner and A. Fery, *J. Polym. Sci., Part B: Polym. Phys.* **54** (23), 2418-2424 (2016).
12. L. Fang, O. E. C. Gould, L. Lysyakova, Y. Jiang, T. Sauter, O. Frank, T. Becker, M. Schossig, K. Kratz and A. Lendlein, *Chemphyschem* **19** (16), 2078-2084 (2018).
13. Q. Zhang, T. Rudolph, A. J. Benitez, O. E. C. Gould, M. Behl, K. Kratz and A. Lendlein, *Smart Mater. Struct.* **28** (5), 055037 (2019).
14. M. Behl, K. Kratz, J. Zotzmann, U. Nöchel and A. Lendlein, *Adv. Mater.* **25** (32), 4466-4469 (2013).
15. X. Wang, H. Zhao, L.-S. Turng and Q. Li, *Ind. Eng. Chem. Res.* **52** (13), 4939-4949 (2013).